

Quantum logarithmic multifractality

Weitao Chen,^{1,2,3} Olivier Giraud,^{2,3,4} Jiangbin Gong,^{1,2,3,*} and Gabriel Lemarié^{2,3,5,†}

¹*Department of Physics, National University of Singapore, Singapore.*

²*MajuLab, CNRS-UCA-SU-NUS-NTU International Joint Research Unit, Singapore.*

³*Centre for Quantum Technologies, National University of Singapore, Singapore.*

⁴*Université Paris-Saclay, CNRS, LPTMS, 91405 Orsay, France.*

⁵*Laboratoire de Physique Théorique, Université de Toulouse, CNRS, UPS, France.*

(Dated: January 1, 2024)

Through a combination of rigorous analytical derivations and extensive numerical simulations, this work reports an exotic multifractal behavior, dubbed “logarithmic multifractality”, in effectively infinite-dimensional systems undergoing the Anderson transition. In marked contrast to conventional multifractal critical properties observed at finite-dimensional Anderson transitions or scale-invariant second-order phase transitions, in the presence of logarithmic multifractality, eigenstate statistics, spatial correlations, and wave packet dynamics can all exhibit scaling laws which are algebraic in the *logarithm* of system size or time. Our findings offer crucial insights into strong finite-size effects and slow dynamics in complex systems undergoing the Anderson transition, such as the many-body localization transition.

Introduction.— Determining the critical threshold of a continuous phase transition can be challenging. At finite system size, temperature, or time, such transition smoothens into a crossover, lacking singular behavior. While second-order phase transitions benefit from the scale-invariance property to discern their threshold [1], other transitions like Kosterlitz-Thouless (KT) type transitions [2] present additional complexities, including logarithmic finite-size effects [3].

The Anderson localization transition, arising from disorder and interference effects, is a well-studied second-order phase transition in finite dimensions [4, 5]. Researchers have employed various methods to determine the critical point [6–24]. Central to this line of research, quantum multifractality is understood as one key property depicting strong and scale-invariant spatial fluctuations of eigenstates at the critical point [25–27]. The said quantum multifractality is investigated by moments $P_q \equiv \sum_i |\psi(i)|^{2q}$ of order q of on-site eigenstate amplitudes $|\psi(i)|^2$ exhibiting an algebraic scaling behavior $P_q \sim N^{-D_q(q-1)}$ with the system size N . While $D_q = 1$ for ergodic delocalization and $D_q = 0$ for localization, D_q for multifractal eigenstates is a non-trivial function of q with $0 < D_q < 1$.

Recently, there has been considerable interest in the Anderson transition in infinite dimensionality (AT^∞), e.g., on random graphs, due to its analogy with the many-body localization (MBL) transition [14, 28–56]. There is an ongoing debate regarding the critical disorder value (even its existence) beyond which eigenstates become many-body localized [57–70]. Addressing this debate presents an outstanding question due to subtle and unavoidable finite-size effects and slow dynamics present in both the MBL transition and the AT^∞ [49, 67]. A complete understanding of finite-size effects and slow dynamics necessitates a thorough study of quantum multifractality in complex systems.

One of the critical features of the AT^∞ is its exotic multifractal properties, characterized by $D_q = 0$ for $q > q^*$ and $D_q > 0$ for $q < q^*$ [4], with a threshold $q^* = \frac{1}{2}$ [71–74]. However, the condition $D_q = 0$ for $q > q^*$ does not reliably identify the transition point, as knowledge of *how* D_q vanishes with system size is essential. For random regular and Erdős-Rényi graphs, it has been shown analytically that $P_2 \sim (\ln N)^{-1/2} + P_2^{N=\infty}$, where $P_2^{N=\infty} > 0$ signifies true localization behavior in the thermodynamic limit [30, 31, 46, 55, 56]. This type of critical behavior is termed “critical localization”. By contrast, numerical simulations have suggested another possibility where P_2 is algebraic in $\ln N$, also compatible with $D_2 = 0$ [39, 50, 52, 75]. This behavior hints at the possibility of $P_q \sim (\ln N)^{f(q)}$, namely, a power function of $\ln N$ with a q -dependent exponent $f(q)$. This second scaling behavior is dubbed below “logarithmic (or log-) multifractality”.

Distinguishing between the above-mentioned two critical behaviors is crucial. Critical localization resembles a Kosterlitz-Thouless (KT) behavior in terms of P_2 : Throughout the localized phase, $P_2^{N=\infty}$ remains finite until a sudden drop to zero in the delocalized phase, accompanied by characteristic logarithmic finite-size effects at the transition [46]. Markedly different, log-multifractality entails the following scenario: localized wave functions on tree-like graphs explore only a few rare branches [39, 50, 52]. This support spans $\ln N$ sites. At the transition, wavefunctions become multifractal on this support. This represents a log-scale invariance not yet explored, to the best of our knowledge.

Based on both analytical and numerical simulations, the present work demonstrates the existence of log-multifractality. Our starting points are the Power-law Random Banded Matrix (PRBM) ensemble [76–78] and the Ruijsenaars-Schneider (RS) ensemble [79–81], previously introduced to explore quantum multifractality thanks to their amenability to analytical treatment

[18, 19, 76–86]. Existing efforts have focused on developing various random matrix ensembles to capture some aspects of AT^∞ . Investigations of variants of the Rosenzweig-Porter model have revealed multifractal phases and slow dynamics [87–97]. However, so far these models fall short of capturing the spatial properties of eigenstates crucial to describe delocalization-localization transition [97]. For our purpose here we introduce a variant of the PRBM ensemble [76, 77] by incorporating a specific decay of the off-diagonal matrix elements. To facilitate our extensive numerical simulations, we also introduce a unitary model akin to the so-called kicked rotor and RS models [80, 81, 98]. Also amenable to analytical treatment, the unitary model introduced here allows us to reach very large system sizes and therefore to investigate dynamical evolution in the regime required to validate the predicted log-multifractal properties. After validating log-multifractality through the algebraic behavior of P_2 in $\ln N$ both analytically and numerically, we explore the slow decay of eigenstate spatial correlations and derive characteristics of wave packet dynamics. As one remarkable consequence of log-multifractality, we find that the return probability exhibits an algebraic decay with $\ln t$ rather than with the time variable t itself.

Models.— We start with the construction of a variant of the PRBM ensemble, namely, the Strongly-multifractal Random Banded Matrix (SRBM) ensemble, defined as an ensemble of $N \times N$ Hermitian matrices \hat{H} whose entries H_{ij} are independent Gaussian random variables with mean $\langle H_{ij} \rangle = 0$ and variance $\langle |H_{ij}|^2 \rangle = \beta^{-1}$ for $i = j$ and

$$\langle |H_{ij}|^2 \rangle = \frac{1}{1 + [|i - j| \ln(1 + |i - j|)/b]^2} \quad (1)$$

for $i \neq j$. Here β is the Dyson index for the orthogonal ($\beta = 1$) and unitary ($\beta = 2$) classes, and $b > 0$ is a real parameter. To mitigate boundary effects in numerical simulations, we replace the term $|i - j|$ with $\sin(\pi|i - j|/N)/(\pi/N)$. In the limit $|i - j| \gg b$, the amplitude (standard deviation) of the off-diagonal elements decays as

$$\sqrt{\langle |H_{ij}|^2 \rangle} \simeq b(|i - j| \ln |i - j|)^{-1}. \quad (2)$$

The decay behavior in Eq. (2) represents the limiting case $a \rightarrow 1, a > 1$, of the PRBM ensemble, where $\sqrt{\langle |H_{ij}|^2 \rangle} \simeq (b/|i - j|)^a$ and the critical value $a = 1$ distinguishes between a delocalized phase ($a < 1$) and a localized phase ($a > 1$) (more precisely a non-critical strongly multifractal phase with $q^* < \frac{1}{2}$) [74]. Indeed we have $\lim_{\epsilon \rightarrow 0} |i - j|^{1+\epsilon} \simeq |i - j|(1 + \epsilon \ln |i - j|)$ for $\epsilon \ll 1$, that is, the decay behavior (2) of the far-off-diagonal elements of SRBM can be roughly understood as the result of keeping the first-order term in $\ln |i - j|$ when taking the $a = 1 + 0^+$ limit of the PRBM. The long-range decay described by Eq. (2) with logarithmic dependence

on $|i - j|$ will be seen to play a pivotal role in inducing log-multifractality.

In addition to the above random Hermitian matrix ensemble, we also consider a unitary ensemble, named Strongly-multifractal Random Unitary Matrix (SRUM) ensemble. The SRUM ensemble can be seen as a variant of the so-called kicked rotor model in quantum chaos and the RS models [80, 81, 98–100]. The SRUM ensemble is comprised of random unitary matrices

$$U_{ij} = e^{i\Phi_i} \sum_{k=1}^N F_{ik} e^{-iKV(2\pi k/N)} F_{kj}^{-1}, \quad (3)$$

where $V(x) = \ln[-1/\ln(\lambda|\sin \frac{x}{2}|)]$ for $x \in [0, 2\pi)$, $V(x + 2\pi) = V(x)$ and the Fourier transform $F_{jk} = e^{2i\pi jk/N}/\sqrt{N}$. The parameter λ is set to $\lambda = 0.9$ to avoid the singularity of $V(x)$ at $x = \pi$. Φ_i are random phases uniformly distributed over $[0, 2\pi)$. Due to the singular behavior of $V(x)$ when $x \rightarrow 0$ (2π), the amplitudes of the matrix elements of U_{ij} decay as $|U_{ij}| \simeq K/(2r \ln r)$ for large $r \equiv |i - j|$; this is the same behavior as $\sqrt{\langle |H_{ij}|^2 \rangle}$ in Eq. (2) with b replaced by $K/2$. This is a further justification of why we have used a singular $V(x)$ as above.

Log-multifractality.— To examine how log-multifractality might emerge in systems with long-range coupling, we analytically compute $\langle P_q \rangle$ by treating the off-diagonal matrix elements in SRBM and SRUM models as perturbation [80, 81]. In the case of SRUM, the unperturbed matrix is diagonal and at order zero eigenstates are $|\psi_i^0\rangle = |i\rangle$. At first order in K , eigenfunctions are given by $|\psi_i^1\rangle = |i\rangle + \sum_{i \neq j} |j\rangle U_{ji}/(e^{i\Phi_i} - e^{i\Phi_j})$. The moments P_q then read

$$\langle P_q \rangle \simeq 1 + \sum_{i \neq j} \langle |e^{i\Phi_i} - e^{i\Phi_j}|^{-2q} \rangle |U_{ij}|^{2q}. \quad (4)$$

Disorder averaging can be performed as $\langle |e^{i\Phi_i} - e^{i\Phi_j}|^{-2q} \rangle = (2\pi)^{-1} \int_0^{2\pi} |1 - e^{i\phi}|^{-2q} d\phi$. For $q < \frac{1}{2}$, this integral converges and Eq. (4) yields

$$\langle P_q \rangle \simeq 1 + K^{2q} A_q (\ln N)^{-2q} N^{-D_q(q-1)}, \quad D_q = \frac{2q-1}{q-1} \quad (5)$$

with A_q a constant. For large N , we approach the conventional multifractal behavior $P_q \sim N^{-D_q(q-1)}$.

Importantly, the above disorder averaging diverges when $q > \frac{1}{2}$, necessitating more advanced treatments. In this context, we employ Levitov renormalization [82, 83], known for its effectiveness in the PRBM and RS ensembles [77, 80]. This approach considers contributions from all 2×2 sub-matrices of U . By calculating the first-order contribution in this manner, disorder averaging converges, yielding the following expression for $q > \frac{1}{2}$:

$$\langle P_q \rangle \sim (\ln N)^{-d_q(q-1)}, \quad d_q = \frac{K\Gamma(q - \frac{1}{2})}{\sqrt{\pi}\Gamma(q-1)(q-1)}. \quad (6)$$

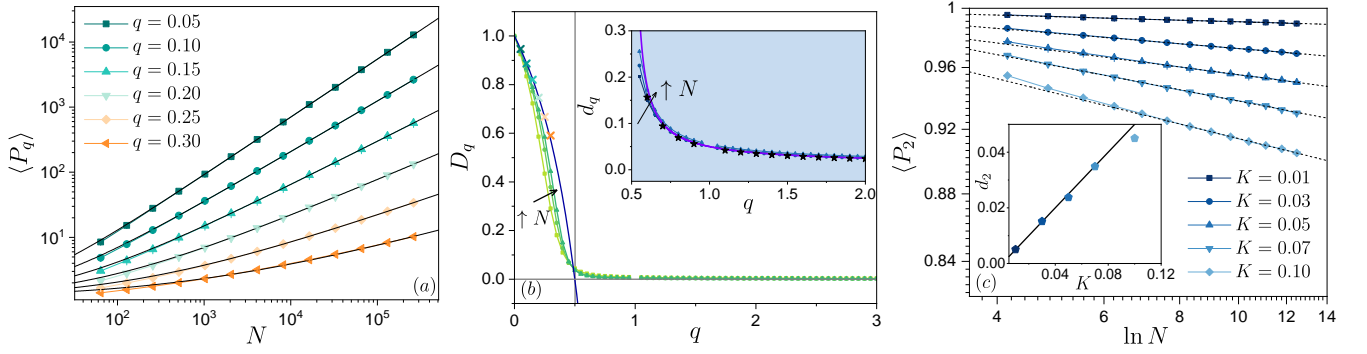


FIG. 1. Eigenstate multifractality in the SRUM model. (a) Conventional multifractality for moments P_q with $q < \frac{1}{2}$ as predicted by Eq. (5) for $K = 0.05$ and different q values as indicated by the labels. The black dashed lines are fits by Eq. (5) with A_q and D_q two fitting parameters. (b) Multifractal dimension D_q vs q for $K = 0.05$. The finite-size estimate $D_q \equiv [\log_2 \langle P_q(N/2) \rangle - \log_2 \langle P_q(N) \rangle] / [q - 1]$, represented by green symbols (lines are an eyeguide) for system sizes $N = 2^{10}, 2^{14}, 2^{18}$, converges slowly to the theoretical prediction $D_q = (2q - 1)/(q - 1)$ for $q < 1/2$. The crosses indicate the D_q values obtained from the fits from Eq. (5) represented in panel (a), which incorporate the log-corrections and agree perfectly well with $D_q = (2q - 1)/(q - 1)$. Inset: Log-multifractal dimension d_q (computed as $[\ln \langle P_q(N/2) \rangle - \ln \langle P_q(N) \rangle] / [(q - 1)(\ln \ln N - \ln \ln \frac{N}{2})]$) as a function of q for system sizes $N = 2^{10}, 2^{14}, 2^{18}$. d_q converges at large N to the non-trivial analytical law (6) (violet line). Star symbols are fitted d_q values shown in panel (c). (c) Log-multifractality for moments with $q > \frac{1}{2}$, well described by Eq. (6). Different curves correspond to different K values as indicated by the labels. The black dashed lines are power-law fits $\langle P_2 \rangle = c(\ln N)^{-d_2}$ with c and d_2 two fitting parameters. Inset: Comparison of the log-multifractal dimension d_2 obtained from fitting (symbols) and the analytical prediction Eq. (6) (black solid line). Disorder averaging ranges from 360,000 realizations for $N = 2^6$ to 1,800 realizations for $N = 2^{18}$. Error bars are smaller than symbol size.

Similar treatments apply to SRBM [101]. For the orthogonal class ($\beta = 1$), we find that $\langle P_q \rangle$ is given by Eq. (5) for $q < \frac{1}{2}$ and Eq. (6) for $q > \frac{1}{2}$, with K replaced by $4b$. In this regard, results from SRUM and SRBM fully echo with each other. Equation (6) shows that our models display log-multifractality, as P_q algebraically scales with $\ln N$ rather than N , and provides an explicit expression for the corresponding multifractal exponent.

To validate the analytical predictions (5)–(6), especially the algebraic behavior in $\ln N$, reaching large system sizes is essential. This is much easier to achieve in the SRUM case. Indeed, implementing a sparse diagonalization approach assisted by a polynomial filter [102], we are able to explore system sizes as large as $N = 2^{18}$ with high number of random realizations. In Fig. 1, the left panel illustrates the conventional multifractal behavior of moments P_q with $q < \frac{1}{2}$, fitting well with Eq. (5). The multifractal dimension D_q is displayed as a function of q in the middle panel, vanishing for $q > \frac{1}{2}$. The right panel showcases the log-multifractality of moments P_q with $q > \frac{1}{2}$, fitting effectively with Eq. (6). The log-multifractal dimension d_q exhibits a non-trivial dependency on q and K , well-accounted for by Eq. (6). These results are also verified for SRBM case [101], albeit at a higher computational cost.

We now turn to the average correlation function of eigenstates, $C(r) \equiv \langle \sum_{i=1}^N |\psi(i)|^2 |\psi(i+r)|^2 \rangle$, a key multifractality probe. It exhibits an exotic behavior given by $C(r) \sim (1/r) \times (\ln r)^{-\alpha}$, with $0 < \alpha < 1$. This behavior, depicted in Fig. 2(b) (red curve) is a distinctive

consequence of log-multifractality when compared with $C(r) \sim r^{D_2-1}$ found in conventional multifractality [4]. This is further illustrated in Figs. S1 and S2 of the Supplementary Material [103]. To roughly explain how these two different correlation functions differ from each other, some additional results suggest that the fractional power function of r^{D_2-1} in conventional multifractal cases is replaced by a power function of $\ln r$ to reflect multifractality in $\ln N$ (Eq. (6)). The additional $1/r$ factor in the $C(r)$ obtained here further indicates nontrivial wavefunction support. More analysis on this side finding will be presented elsewhere [101].

Wave packet dynamics.— The dynamics of a wave packet initialized at a single site $\psi(r, t = 0) = \delta_{r,0}$ also encodes rich information on quantum multifractality [18, 21, 23, 24, 104]. In the context of conventional multifractality, the return probability $R_0(t) \equiv |\langle \psi(t) | \psi(0) \rangle|^2$ exhibits a power-law decay with time t , $\langle R_0 \rangle \sim t^{-D_2}$, with an exponent given by the multifractal dimension D_2 [17–19]. To analyze $R_0(t)$ in the case of log-multifractality, we focus on the orthogonal SRBM model with Dyson index $\beta = 1$. We adapt the analytic expression for the return probability that was obtained for the PRBM case in the limit $b \ll 1$ by means of a supersymmetric virial expansion [19] $\langle R_0 \rangle = \langle R_0^{(0)} \rangle + \langle R_0^{(1)} \rangle + \dots$ in terms of successive orders of the parameter b , with $\langle R_0^{(0)} \rangle = 1$. Adapting Eq. (B.1) of [19] to our SRBM ensemble, we

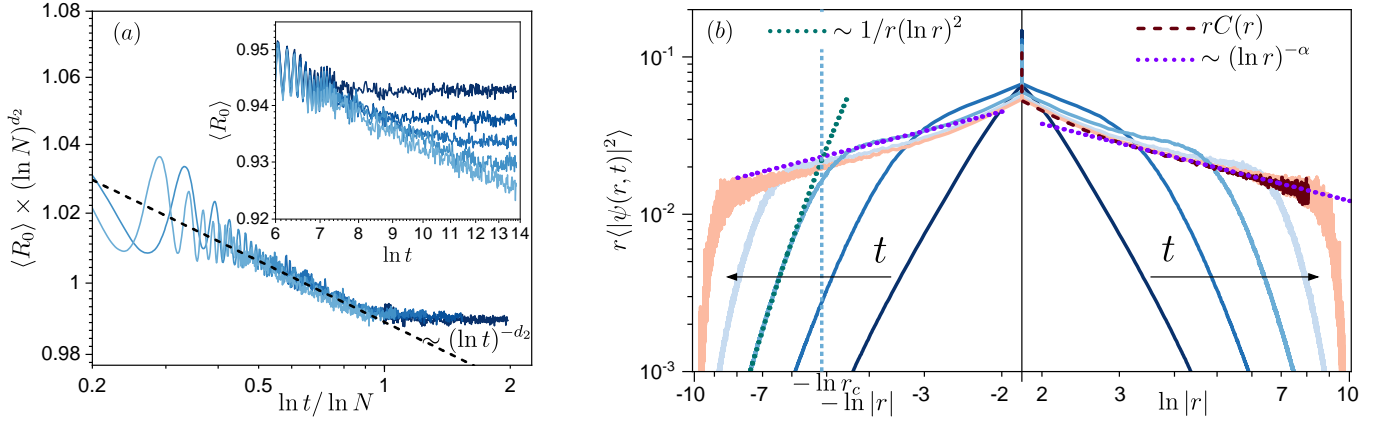


FIG. 2. Slow wave packet dynamics for the SRUM with initial state $\psi(r, t=0) = \delta_{r,0}$, in connection with log-multifractality. (a) Illustration of the scaling property in Eq. (8) for the return probability $\langle R_0 \rangle$ at $K = 0.05$. The data from various system sizes and times $t \in [10, 10^6]$ collapse onto a single scaling curve when $\langle R_0 \rangle \times (\ln N)^{d_2}$ is plotted against the scaled time $\ln t / \ln N$. The black dashed line represents a power-law fit, $\langle R_0 \rangle \sim (\ln t)^{-d_2}$, giving $d_2 \approx 0.025$ in perfect agreement with the analytical prediction $d_2 = K/2$ and the value extracted from P_2 . Inset: corresponding raw data for $\langle R_0 \rangle$ with, from top to bottom, $N = 2^7, 2^9, \dots, 2^{15}$. Results are averaged over a range from 18,000 realizations for $N = 2^7$ to 7,200 realizations for $N = 2^{15}$. (b) Average probability distribution of the wave packet at different times plotted as $r \langle |\psi(r, t)|^2 \rangle$ vs. $\ln r$ in a symmetrical log-log scale, with $K = 1.0$. Curves from dark blue to pale orange correspond to evolution times $t = 10, 77, 1668, 35398, 10^5$. The violet dotted line fits the behavior expected at short distances $r \ll r_c$, corresponding to the correlation function $C(r)$ (shown by the maroon dashed line), giving $\alpha \approx 0.7$; while the green dotted line fits the one for $r \gg r_c$, see Eq. (9). The vertical dashed line locates the crossover r_c . Results are averaged over 720,000 (36,000 for $C(r)$) disorder configurations with system size $N = 2^{15}$ ($N = 2^{16}$ for $C(r)$).

arrive at

$$\langle R_0^{(1)} \rangle = -\frac{\sqrt{2\pi}}{N} \sum_{i \neq j}^N e^{-2b_{ij}t^2} 2b_{ij}|t| I_0(2b_{ij}t^2), \quad (7)$$

where $b_{ij} = \frac{1}{2} \langle |H_{ij}|^2 \rangle \simeq \frac{b^2}{2(|i-j| \ln |i-j|)^2}$ and $I_0(x)$ is the 0th order modified Bessel function. In the large N limit, we can replace the sum in Eq. (7) by an integral. Since $\ln \langle R_0 \rangle \simeq \langle R_0^{(1)} \rangle$, a direct calculation yields $-\partial \langle R_0^{(1)} \rangle / \partial \ln \ln t \simeq_{t \rightarrow \infty} 2b$, which coincides with the value of d_2 calculated above for SRBM. Hence, $\langle R_0 \rangle \sim (\ln t)^{-d_2}$, which indicates an algebraic decay of $\langle R_0 \rangle$ in $\ln t$ controlled by the log-multifractal dimension d_2 . On the other hand, for a finite size N , the limit $t \rightarrow \infty$ gives $\langle R_0 \rangle \sim \langle P_2 \rangle \sim (\ln N)^{-d_2}$ (see Eq. (6)). Therefore, there must exist a characteristic time scale t^* separating the infinite-size behavior $\sim (\ln t)^{-d_2}$ of $\langle R_0 \rangle$ from its finite-size stationary value $\sim (\ln N)^{-d_2}$, with $\ln t^* \sim \ln N$. We can hence assume, as was done in [24], the following scaling behavior:

$$\langle R_0(t, N) \rangle = (\ln N)^{-d_2} g(\ln t / \ln N), \quad (8)$$

with $g(x) \sim_{x \ll 1} x^{-d_2}$ and $g(x) \sim_{x \gg 1} \text{cst.}$ The same scaling behavior is expected for SRUM ensemble, as the amplitudes of its off-diagonal elements decay in the same way. The results, shown in Fig. 2(a) for SRUM, confirm the validity of the scaling described by Eq. (8).

It is also interesting to examine the spatial expansion of a time-evolving wave packet. In the long-time limit or for sufficiently small r , we find that the wave packet amplitudes exhibit a decay behavior similar to the average spatial correlation function of the eigenstates, $C(r)$. In the short-time limit or for sufficiently large r , the wave packet amplitudes decay following, instead, the direct long-range couplings described by the off-diagonal matrix elements, i.e., Eq. (2). If we introduce r_c as the crossover scale between the two regimes, these two behaviors can be summarized as

$$\langle |\psi(r, t)|^2 \rangle = \begin{cases} \langle R_0 \rangle [r(\ln r)^\alpha]^{-1}, & 1 < r < r_c, \\ B \left[\frac{r}{r_c} \ln \left(\frac{r}{r_c} \right) \right]^{-2}, & r_c < r \leq \frac{N}{2}, \end{cases} \quad (9)$$

with $B = \langle R_0 \rangle [r_c(\ln r_c)^\alpha]^{-1}$ [23, 24, 104–106].

Generalization to critical localization.— We can construct a whole family of SRBM ensembles if we replace the logarithmic function in Eq. (1) by $\ln^{1+\mu}$ with $\mu \geq 0$. The parameter μ influences various properties and behaviors of the system. If we focus on the case of $q = 2$ only, analytical procedures as above for $\mu > 0$ lead to $\langle P_2 \rangle \sim (\ln N)^{-\mu} + P_2^{N=\infty}$, with $P_2^{N=\infty} > 0$ indicative of a localization behavior. Our numerical observations also reveal that the spatial correlation function of the eigenstates decays as $C(r) \sim 1/[r(\ln r)^{1+\mu}]$ (see Fig. S3 of the Supplementary Material [103]). Noteworthy is that when $\mu = \frac{1}{2}$ both of these results align with the analytical predictions for the Anderson model on random regular and

Erdős-Rényi graphs [30, 31, 46]. This suggests a potential connection between the free parameter μ and the specific characteristics of certain types of graphs.

Conclusion.— In this Letter, we have presented, both analytically and computationally, compelling evidence of log-multifractality at the Anderson transition of effective infinite-dimensionality, through the scaling behavior $\langle P_q \rangle \sim (\ln N)^{-d_q(q-1)}$ for $q > \frac{1}{2}$. This scaling behavior signifies a remarkable scale invariance in the logarithm of the system size, extending beyond conventional multifractality in finite dimension and scale invariance in second-order phase transitions. Logarithmic multifractality controls the slow decay of spatial correlations and the slow dynamics of a time-evolving wave packet, particularly its return probability $\langle R_0 \rangle \sim (\ln t)^{-d_2}$. Finally, we discussed how to generalize our random matrix models to obtain other “critical localization” scenarios predicted at the Anderson transition points on random regular and Erdős-Rényi graphs [30, 31, 46]. This work thus uncovers distinctive characteristics of the Anderson transition in infinite dimensionality, demonstrating the existence of transition classes beyond those observed so far [52, 53]. Extensions of this work shall offer opportunities to address related challenges, including strong finite-size effects and slow dynamics near the many-body localization transition.

This study was supported by research funding Grants No. ANR-18-CE30-0017 and ANR-19-CE30-0013, and by the Singapore Ministry of Education Academic Research Fund Tier I (WBS No. R-144-000-437-114). We thank Calcul en Midi-Pyrénées (CALMIP) and the National Supercomputing Centre (NSCC) of Singapore for computational resources and assistance. W. Chen is supported by the President’s Graduate Fellowship at National University of Singapore and the Merlion Ph.D. Scholarship awarded by the French Embassy in Singapore.

* phygj@nus.edu.sg

† lemarie@irsamc.ups-tlse.fr

- [1] K. G. Wilson, The renormalization group and critical phenomena, *Rev. Mod. Phys.* **55**, 583 (1983).
- [2] J. M. Kosterlitz, Kosterlitz–Thouless physics: a review of key issues, *Reports on Progress in Physics* **79**, 026001 (2016).
- [3] Y.-D. Hsieh, Y.-J. Kao, and A. W. Sandvik, Finite-size scaling method for the Berezinskii–Kosterlitz–Thouless transition, *Journal of Statistical Mechanics: Theory and Experiment* **2013**, P09001 (2013).
- [4] F. Evers and A. D. Mirlin, Anderson transitions, *Rev. Mod. Phys.* **80**, 1355 (2008).
- [5] E. Abrahams, *50 years of Anderson Localization*, Vol. 24 (world scientific, 2010).
- [6] C. Castellani and L. Peliti, Multifractal wavefunction at the localisation threshold, *Journal of physics A: mathematical and general* **19**, L429 (1986).
- [7] A. Rodriguez, L. J. Vasquez, and R. A. Römer, Multifractal Analysis with the Probability Density Function at the Three-Dimensional Anderson Transition, *Phys. Rev. Lett.* **102**, 106406 (2009).
- [8] S. Faez, A. Strybulevych, J. H. Page, A. Lagendijk, and B. A. van Tiggelen, Observation of Multifractality in Anderson Localization of Ultrasound, *Phys. Rev. Lett.* **103**, 155703 (2009).
- [9] A. Rodriguez, L. J. Vasquez, K. Slevin, and R. A. Römer, Multifractal finite-size scaling and universality at the Anderson transition, *Phys. Rev. B* **84**, 134209 (2011).
- [10] G. Lemarié, J. Chabé, P. Szriftgiser, J. C. Garreau, B. Grémaud, and D. Delande, Observation of the Anderson metal-insulator transition with atomic matter waves: Theory and experiment, *Phys. Rev. A* **80**, 043626 (2009).
- [11] G. Lemarié, H. Lignier, D. Delande, P. Szriftgiser, and J. C. Garreau, Critical State of the Anderson Transition: Between a Metal and an Insulator, *Phys. Rev. Lett.* **105**, 090601 (2010).
- [12] J. Chabé, G. Lemarié, B. Grémaud, D. Delande, P. Szriftgiser, and J. C. Garreau, Experimental Observation of the Anderson Metal-Insulator Transition with Atomic Matter Waves, *Phys. Rev. Lett.* **101**, 255702 (2008).
- [13] E. Cuevas, V. Gasparian, and M. Ortuño, Anomalous Large Critical Regions in Power-Law Random Matrix Ensembles, *Phys. Rev. Lett.* **87**, 056601 (2001).
- [14] E. Tarquini, G. Biroli, and M. Tarzia, Critical properties of the Anderson localization transition and the high-dimensional limit, *Phys. Rev. B* **95**, 094204 (2017).
- [15] T. Ohtsuki and T. Kawarabayashi, Anomalous Diffusion at the Anderson Transitions, *Journal of the Physical Society of Japan* **66**, 314 (1997).
- [16] C. A. Müller, D. Delande, and B. Shapiro, Critical dynamics at the Anderson localization mobility edge, *Phys. Rev. A* **94**, 033615 (2016).
- [17] R. Ketzmerick, G. Petschel, and T. Geisel, Slow decay of temporal correlations in quantum systems with Cantor spectra, *Phys. Rev. Lett.* **69**, 695 (1992).
- [18] V. E. Kravtsov, A. Ossipov, O. M. Yevtushenko, and E. Cuevas, Dynamical scaling for critical states: Validity of Chalker’s ansatz for strong fractality, *Phys. Rev. B* **82**, 161102 (2010).
- [19] V. E. Kravtsov, A. Ossipov, and O. M. Yevtushenko, Return probability and scaling exponents in the critical random matrix ensemble, *Journal of Physics A: Mathematical and Theoretical* **44**, 305003 (2011).
- [20] B. Altshuler and V. Kravtsov, Random Cantor sets and mini-bands in local spectrum of quantum systems, *Annals of Physics* **456**, 169300 (2023).
- [21] S. Ghosh, C. Miniatura, N. Cherroret, and D. Delande, Coherent forward scattering as a signature of Anderson metal-insulator transitions, *Phys. Rev. A* **95**, 041602 (2017).
- [22] M. Martinez, G. Lemarié, B. Georgeot, C. Miniatura, and O. Giraud, Coherent forward scattering as a robust probe of multifractality in critical disordered media, *SciPost Phys.* **14**, 057 (2023).
- [23] P. Akridas-Morel, N. Cherroret, and D. Delande, Multifractality of the kicked rotor at the critical point of the Anderson transition, *Phys. Rev. A* **100**, 043612 (2019).
- [24] W. Chen, G. Lemarié, and J. Gong, Critical dynamics

- of long-range quantum disordered systems, *Phys. Rev. E* **108**, 054127 (2023).
- [25] B. B. Mandelbrot, Intermittent turbulence in self-similar cascades: divergence of high moments and dimension of the carrier, *Journal of fluid Mechanics* **62**, 331 (1974).
- [26] B. B. Mandelbrot and B. B. Mandelbrot, *The fractal geometry of nature*, Vol. 1 (WH freeman New York, 1982).
- [27] K. Falconer, *Fractal geometry: mathematical foundations and applications* (John Wiley & Sons, 2004).
- [28] M. R. Zirnbauer, Localization transition on the Bethe lattice, *Phys. Rev. B* **34**, 6394 (1986).
- [29] M. R. Zirnbauer, Anderson localization and non-linear sigma model with graded symmetry, *Nuclear Physics B* **265**, 375 (1986).
- [30] Y. V. Fyodorov and A. D. Mirlin, Localization in ensemble of sparse random matrices, *Phys. Rev. Lett.* **67**, 2049 (1991).
- [31] A. D. Mirlin and Y. V. Fyodorov, Distribution of local densities of states, order parameter function, and critical behavior near the Anderson transition, *Phys. Rev. Lett.* **72**, 526 (1994).
- [32] C. Monthus and T. Garel, Anderson localization on the Cayley tree: multifractal statistics of the transmission at criticality and off criticality, *Journal of Physics A: Mathematical and Theoretical* **44**, 145001 (2011).
- [33] G. Biroli, A. C. Ribeiro-Teixeira, and M. Tarzia, Difference between level statistics, ergodicity and localization transitions on the Bethe lattice (2012), [arXiv:1211.7334 \[cond-mat.dis-nn\]](#).
- [34] A. De Luca, B. L. Altshuler, V. E. Kravtsov, and A. Scardicchio, Anderson Localization on the Bethe Lattice: Nonergodicity of Extended States, *Phys. Rev. Lett.* **113**, 046806 (2014).
- [35] B. L. Altshuler, E. Cuevas, L. B. Ioffe, and V. E. Kravtsov, Nonergodic Phases in Strongly Disordered Random Regular Graphs, *Phys. Rev. Lett.* **117**, 156601 (2016).
- [36] K. S. Tikhonov, A. D. Mirlin, and M. A. Skvortsov, Anderson localization and ergodicity on random regular graphs, *Phys. Rev. B* **94**, 220203 (2016).
- [37] K. S. Tikhonov and A. D. Mirlin, Fractality of wave functions on a Cayley tree: Difference between tree and locally treelike graph without boundary, *Phys. Rev. B* **94**, 184203 (2016).
- [38] M. Sonner, K. S. Tikhonov, and A. D. Mirlin, Multifractality of wave functions on a Cayley tree: From root to leaves, *Phys. Rev. B* **96**, 214204 (2017).
- [39] I. García-Mata, O. Giraud, B. Georgeot, J. Martin, R. Dubertrand, and G. Lemarié, Scaling Theory of the Anderson Transition in Random Graphs: Ergodicity and Universality, *Phys. Rev. Lett.* **118**, 166801 (2017).
- [40] G. Biroli and M. Tarzia, Delocalized glassy dynamics and many-body localization, *Phys. Rev. B* **96**, 201114 (2017).
- [41] V. Kravtsov, B. Altshuler, and L. Ioffe, Non-ergodic delocalized phase in Anderson model on Bethe lattice and regular graph, *Annals of Physics* **389**, 148 (2018).
- [42] K. S. Tikhonov and A. D. Mirlin, Critical behavior at the localization transition on random regular graphs, *Phys. Rev. B* **99**, 214202 (2019).
- [43] G. De Tomasi, S. Bera, A. Scardicchio, and I. M. Khaymovich, Subdiffusion in the Anderson model on the random regular graph, *Phys. Rev. B* **101**, 100201 (2020).
- [44] G. Parisi, S. Pascazio, F. Pietracaprina, V. Ros, and A. Scardicchio, Anderson transition on the Bethe lattice: an approach with real energies, *Journal of Physics A: Mathematical and Theoretical* **53**, 014003 (2019).
- [45] S. Bera, G. De Tomasi, I. M. Khaymovich, and A. Scardicchio, Return probability for the Anderson model on the random regular graph, *Phys. Rev. B* **98**, 134205 (2018).
- [46] K. S. Tikhonov and A. D. Mirlin, Statistics of eigenstates near the localization transition on random regular graphs, *Phys. Rev. B* **99**, 024202 (2019).
- [47] S. Roy and D. E. Logan, Localization on Certain Graphs with Strongly Correlated Disorder, *Phys. Rev. Lett.* **125**, 250402 (2020).
- [48] G. Biroli, A. K. Hartmann, and M. Tarzia, Critical behavior of the Anderson model on the Bethe lattice via a large-deviation approach, *Phys. Rev. B* **105**, 094202 (2022).
- [49] K. Tikhonov and A. Mirlin, From Anderson localization on random regular graphs to many-body localization, *Annals of Physics* **435**, 168525 (2021), special Issue on Localisation 2020.
- [50] I. García-Mata, J. Martin, R. Dubertrand, O. Giraud, B. Georgeot, and G. Lemarié, Two critical localization lengths in the Anderson transition on random graphs, *Phys. Rev. Res.* **2**, 012020 (2020).
- [51] L. Colmenarez, D. J. Luitz, I. M. Khaymovich, and G. De Tomasi, Subdiffusive Thouless time scaling in the Anderson model on random regular graphs, *Phys. Rev. B* **105**, 174207 (2022).
- [52] I. García-Mata, J. Martin, O. Giraud, B. Georgeot, R. Dubertrand, and G. Lemarié, Critical properties of the Anderson transition on random graphs: Two-parameter scaling theory, Kosterlitz-Thouless type flow, and many-body localization, *Phys. Rev. B* **106**, 214202 (2022).
- [53] C. Vanoni, B. L. Altshuler, V. E. Kravtsov, and A. Scardicchio, Renormalization Group Analysis of the Anderson Model on Random Regular Graphs (2023), [arXiv:2306.14965 \[cond-mat.dis-nn\]](#).
- [54] M. Baroni, G. G. Lorenzana, T. Rizzo, and M. Tarzia, Corrections to the Bethe lattice solution of Anderson localization (2023), [arXiv:2304.10365 \[cond-mat.dis-nn\]](#).
- [55] Y. Fyodorov, A. Mirlin, and H.-J. Sommers, A novel field theoretical approach to the Anderson localization: sparse random hopping model, *Journal de Physique I* **2**, 1571 (1992).
- [56] A. D. Mirlin and Y. V. Fyodorov, Universality of level correlation function of sparse random matrices, *Journal of Physics A: Mathematical and General* **24**, 2273 (1991).
- [57] W. De Roeck and F. m. c. Huveneers, Stability and instability towards delocalization in many-body localization systems, *Phys. Rev. B* **95**, 155129 (2017).
- [58] A. Morningstar, L. Colmenarez, V. Khemani, D. J. Luitz, and D. A. Huse, Avalanches and many-body resonances in many-body localized systems, *Phys. Rev. B* **105**, 174205 (2022).
- [59] D. Sels, Bath-induced delocalization in interacting disordered spin chains, *Phys. Rev. B* **106**, L020202 (2022).
- [60] J. Léonard, S. Kim, M. Rispoli, A. Lukin, R. Schittko, J. Kwan, E. Demler, D. Sels, and M. Greiner, Signatures of bath-induced quantum avalanches in a many-body-localized system (2022), [arXiv:2012.15270 \[cond-](#)

- [mat.quant-gas](#)].
- [61] F. Weiner, F. Evers, and S. Bera, Slow dynamics and strong finite-size effects in many-body localization with random and quasiperiodic potentials, *Phys. Rev. B* **100**, 104204 (2019).
 - [62] J. Šuntajs, J. Bonča, T. c. v. Prosen, and L. Vidmar, Quantum chaos challenges many-body localization, *Phys. Rev. E* **102**, 062144 (2020).
 - [63] J. Šuntajs, J. Bonča, T. c. v. Prosen, and L. Vidmar, Ergodicity breaking transition in finite disordered spin chains, *Phys. Rev. B* **102**, 064207 (2020).
 - [64] M. Kiefer-Emmanouilidis, R. Unanyan, M. Fleischhauer, and J. Sirker, Slow delocalization of particles in many-body localized phases, *Phys. Rev. B* **103**, 024203 (2021).
 - [65] D. Sels and A. Polkovnikov, Dynamical obstruction to localization in a disordered spin chain, *Phys. Rev. E* **104**, 054105 (2021).
 - [66] L. Vidmar, B. Krajewski, J. Bonča, and M. Mierzejewski, Phenomenology of Spectral Functions in Disordered Spin Chains at Infinite Temperature, *Phys. Rev. Lett.* **127**, 230603 (2021).
 - [67] D. Abanin, J. Bardarson, G. De Tomasi, S. Gopalakrishnan, V. Khemani, S. Parameswaran, F. Pollmann, A. Potter, M. Serbyn, and R. Vasseur, Distinguishing localization from chaos: Challenges in finite-size systems, *Annals of Physics* **427**, 168415 (2021).
 - [68] P. Sierant, D. Delande, and J. Zakrzewski, Thouless Time Analysis of Anderson and Many-Body Localization Transitions, *Phys. Rev. Lett.* **124**, 186601 (2020).
 - [69] R. K. Panda, A. Scardicchio, M. Schulz, S. R. Taylor, and M. Žnidarič, Can we study the many-body localisation transition?, *Europhysics Letters* **128**, 67003 (2020).
 - [70] D. J. Luitz and Y. B. Lev, Absence of slow particle transport in the many-body localized phase, *Phys. Rev. B* **102**, 100202 (2020).
 - [71] A. D. Mirlin, Y. V. Fyodorov, A. Mildenberger, and F. Evers, Exact Relations between Multifractal Exponents at the Anderson Transition, *Phys. Rev. Lett.* **97**, 046803 (2006).
 - [72] I. A. Gruzberg, A. W. W. Ludwig, A. D. Mirlin, and M. R. Zirnbauer, Symmetries of multifractal spectra and field theories of Anderson localization, *Phys. Rev. Lett.* **107**, 086403 (2011).
 - [73] I. A. Gruzberg, A. D. Mirlin, and M. R. Zirnbauer, Classification and symmetry properties of scaling dimensions at Anderson transitions, *Phys. Rev. B* **87**, 125144 (2013).
 - [74] A. M. Bilen, B. Georgeot, O. Giraud, G. Lemarié, and I. García-Mata, Symmetry violation of quantum multifractality: Gaussian fluctuations versus algebraic localization, *Phys. Rev. Res.* **3**, L022023 (2021).
 - [75] A. Chen, J. Maciejko, and I. Boettcher, Anderson localization transition in disordered hyperbolic lattices (2023), [arXiv:2310.07978 \[cond-mat.dis-nn\]](#).
 - [76] A. D. Mirlin, Y. V. Fyodorov, F.-M. Dittes, J. Quezada, and T. H. Seligman, Transition from localized to extended eigenstates in the ensemble of power-law random banded matrices, *Phys. Rev. E* **54**, 3221 (1996).
 - [77] A. D. Mirlin and F. Evers, Multifractality and critical fluctuations at the Anderson transition, *Phys. Rev. B* **62**, 7920 (2000).
 - [78] E. Bogomolny and M. Sieber, Power-law random banded matrices and ultrametric matrices: Eigenvalue distribution in the intermediate regime, *Phys. Rev. E* **98**, 042116 (2018).
 - [79] E. Bogomolny, O. Giraud, and C. Schmit, Random Matrix Ensembles Associated with Lax Matrices, *Phys. Rev. Lett.* **103**, 054103 (2009).
 - [80] E. Bogomolny and O. Giraud, Perturbation approach to multifractal dimensions for certain critical random-matrix ensembles, *Phys. Rev. E* **84**, 036212 (2011).
 - [81] E. Bogomolny and O. Giraud, Multifractal dimensions for all moments for certain critical random-matrix ensembles in the strong multifractality regime, *Phys. Rev. E* **85**, 046208 (2012).
 - [82] L. S. Levitov, Absence of Localization of Vibrational Modes Due to Dipole-Dipole Interaction, *Europhysics Letters* **9**, 83 (1989).
 - [83] L. S. Levitov, Delocalization of vibrational modes caused by electric dipole interaction, *Phys. Rev. Lett.* **64**, 547 (1990).
 - [84] C. Monthus and T. Garel, The Anderson localization transition with long-ranged hoppings: analysis of the strong multifractality regime in terms of weighted Lévy sums, *Journal of Statistical Mechanics: Theory and Experiment* **2010**, P09015 (2010).
 - [85] E. Bogomolny and O. Giraud, Eigenfunction Entropy and Spectral Compressibility for Critical Random Matrix Ensembles, *Phys. Rev. Lett.* **106**, 044101 (2011).
 - [86] O. Yevtushenko and A. Ossipov, A supersymmetry approach to almost diagonal random matrices, *Journal of Physics A: Mathematical and Theoretical* **40**, 4691 (2007).
 - [87] V. E. Kravtsov, I. M. Khaymovich, E. Cuevas, and M. Amini, A random matrix model with localization and ergodic transitions, *New Journal of Physics* **17**, 122002 (2015).
 - [88] G. D. Tomasi, M. Amini, S. Bera, I. M. Khaymovich, and V. E. Kravtsov, Survival probability in Generalized Rosenzweig-Porter random matrix ensemble, *SciPost Phys.* **6**, 014 (2019).
 - [89] I. M. Khaymovich, V. E. Kravtsov, B. L. Altshuler, and L. B. Ioffe, Fragile extended phases in the log-normal Rosenzweig-Porter model, *Phys. Rev. Res.* **2**, 043346 (2020).
 - [90] P. von Soosten and S. Warzel, Non-ergodic delocalization in the Rosenzweig–Porter model, *Letters in Mathematical Physics* **109**, 905 (2019).
 - [91] K. Truong and A. Ossipov, Eigenvectors under a generic perturbation: Non-perturbative results from the random matrix approach, *Europhysics Letters* **116**, 37002 (2016).
 - [92] E. Bogomolny and M. Sieber, Eigenfunction distribution for the Rosenzweig-Porter model, *Phys. Rev. E* **98**, 032139 (2018).
 - [93] C. Monthus, Multifractality of eigenstates in the delocalized non-ergodic phase of some random matrix models: Wigner–Weisskopf approach, *Journal of Physics A: Mathematical and Theoretical* **50**, 295101 (2017).
 - [94] M. Amini, Spread of wave packets in disordered hierarchical lattices, *Europhysics Letters* **117**, 30003 (2017).
 - [95] G. Biroli and M. Tarzia, Lévy-Rosenzweig-Porter random matrix ensemble, *Phys. Rev. B* **103**, 104205 (2021).
 - [96] V. E. Kravtsov, I. M. Khaymovich, B. L. Altshuler, and L. B. Ioffe, Localization transition on the random regular graph as an unstable tricritical point in a log-normal rosenzweig-porter random matrix ensemble

- (2020), [arXiv:2002.02979 \[cond-mat.dis-nn\]](#).
- [97] I. M. Khaymovich and V. E. Kravtsov, Dynamical phases in a “multifractal” Rosenzweig-Porter model, [SciPost Phys. **11**, 045 \(2021\)](#).
 - [98] A. M. García-García and J. Wang, Anderson Transition in Quantum Chaos, [Phys. Rev. Lett. **94**, 244102 \(2005\)](#).
 - [99] B. V. Chirikov, A universal instability of many-dimensional oscillator systems, [Physics Reports **52**, 263 \(1979\)](#).
 - [100] F. M. Izrailev, Simple models of quantum chaos: Spectrum and eigenfunctions, [Physics Reports **196**, 299 \(1990\)](#).
 - [101] W. Chen, O. Giraud, J. Gong, and G. Lemarié, In Preparation, (2024).
 - [102] D. J. Luitz, Polynomial filter diagonalization of large Floquet unitary operators, [SciPost Phys. **11**, 021 \(2021\)](#).
 - [103] See Supplemental Material.
 - [104] V. E. Kravtsov, O. M. Yevtushenko, P. Snajberk, and E. Cuevas, Lévy flights and multifractality in quantum critical diffusion and in classical random walks on fractals, [Phys. Rev. E **86**, 021136 \(2012\)](#).
 - [105] R. Ketzmerick, K. Kruse, S. Kraut, and T. Geisel, What Determines the Spreading of a Wave Packet?, [Phys. Rev. Lett. **79**, 1959 \(1997\)](#).
 - [106] J. Chalker, Scaling and eigenfunction correlations near a mobility edge, [Physica A: Statistical Mechanics and its Applications **167**, 253 \(1990\)](#).

Supplemental Material for “Quantum logarithmic multifractality”

I. NUMERICAL RESULTS FOR THE CORRELATION FUNCTION

In this section, we present numerical results for the correlation function

$$C(r) \equiv \left\langle \sum_{i=1}^N |\psi_j(i)|^2 |\psi_j(i+r)|^2 \right\rangle \quad (\text{S1})$$

of the SRBM model and the SRUM model. In (S1) we perform averaging on both disorder realizations and eigenstates ψ_j . The numerical results displayed in Fig. S1 and Fig. S2 support our argument of the spatial decay behavior

$$C(r) \sim \frac{1}{r(\ln r)^\alpha}. \quad (\text{S2})$$

We find that the decay exponent α is related to the log-multifractal dimension d_2 by $\alpha + d_2 \approx 1$ in the SRBM model. However, such a relationship is absent in the SRUM model.

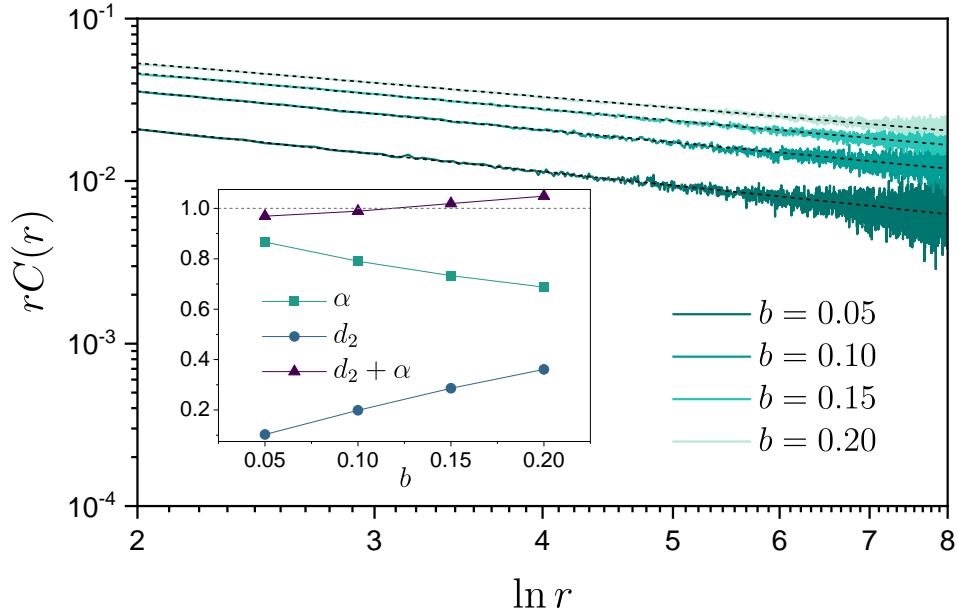


FIG. S1. Spatial decay of the correlation function $C(r)$ Eq. (S2) in the SRBM model for different b values as indicated by the labels. The data is plotted as $rC(r)$ a function of $\ln r$ in log-log scale, the dash lines are power-law fits $rC(r) \sim (\ln r)^{-\alpha}$. Results have been averaged over 18,000 realizations with $N = 2^{14}$. Inset: Verification of the relationship $d_2 + \alpha = 1$.

II. NUMERICAL RESULTS FOR THE GENERALIZED SRBM MODEL

In this section, we present numerical results for the generalized SRBM model with parameter $\mu = 1/2$. From analytic considerations (see main text), we expect a localized behavior of the inverse participation ratio

$$\langle P_2 \rangle \sim (\ln N)^{-\mu} + \text{cst}. \quad (\text{S3})$$

and a spatial decay of the correlation function following

$$C(r) \sim \frac{1}{r(\ln r)^{1+\mu}}. \quad (\text{S4})$$

Numerical results presented in Fig. S3 validate the above predictions.

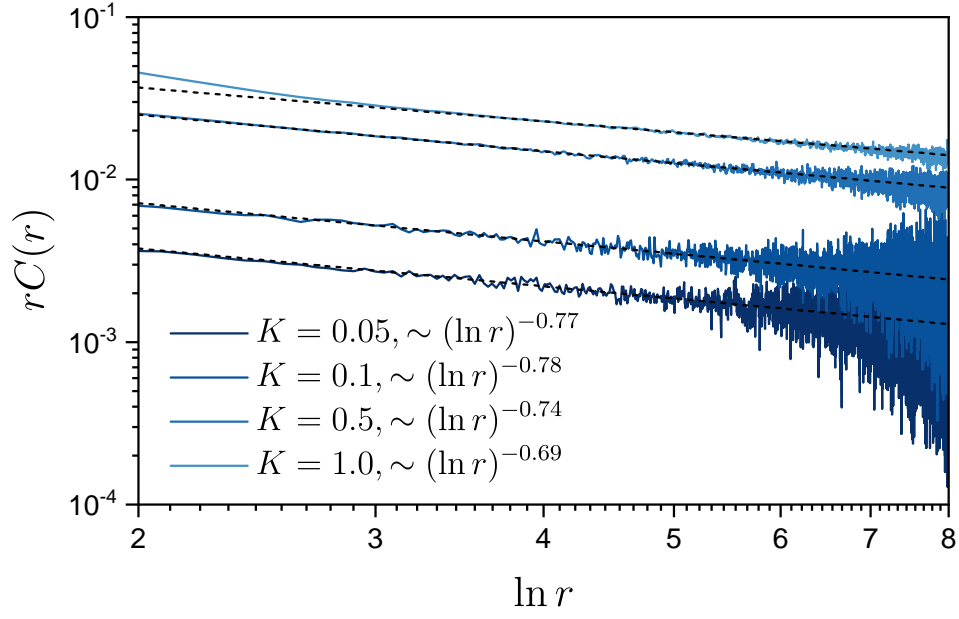


FIG. S2. Spatial decay for the correlation function $C(r)$ Eq. (S2) in the SRUM model for different K values as indicated by the labels. The data is plotted as $rC(r)$ a function of $\ln r$ in log-log scale, the dash lines are power-law fittings $rC(r) \sim (\ln r)^{-\alpha}$. Results have been averaged over 36,000 realizations with $N = 2^{16}$.

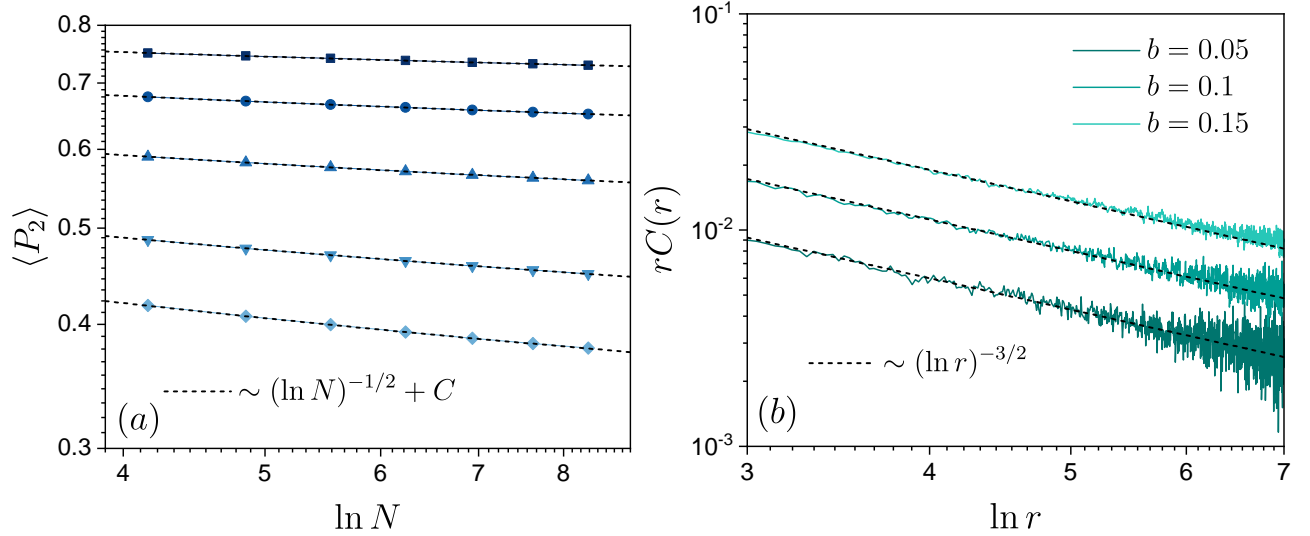


FIG. S3. (a) Scaling property Eq. (S3) for the generalized SRBM model with $\mu = 1/2$; different curves correspond to different b values: $b = 0.05, 0.07, 0.1, 0.15, 0.2$ from top to bottom. The black dashed lines are power-law fits $\langle P_2 \rangle \sim (\ln N)^{-\mu} + C$. Disorder averaging ranges from 360,000 realizations for $N = 2^6$ to 18,000 realizations for $N = 2^{12}$. (b) Spatial decay for the correlation function $C(r)$ Eq. (S4) in the generalized SRBM model with $\mu = 1/2$ for different b values as indicated by the labels. The data is plotted as $rC(r)$ a function of $\ln r$ in log-log scale, the dash lines are power-law fittings $rC(r) \sim (\ln r)^{-(1+\mu)}$. Results have been averaged over 18,000 realizations with $N = 2^{14}$.